Available online at www.sciencedirect.com
ScienceDirect
Magnetic Resonance Imaging 28 (2010) 1395–1402
MAGNETIC RESONANCE IMAGING

Original contributions

Three dimension double inversion recovery gray matter imaging using compressed sensing

Sung-Min Gho[a], Yoonho Nam[a], Sang-Young Zho[a], Eung Yeop Kim[b], Dong-Hyun Kim[a,b,*]

[a]Department of Electrical and Electronic Engineering, Yonsei University, 134 Sinchon-dong, Seodaemun-gu, Seoul 120-749, South Korea
[b]Department of Radiology, Research Institute of Radiological Science, Yonsei University College of Medicine, Seodaemun-gu, Seoul 120-752, South Korea

Received 27 January 2010; revised 24 May 2010; accepted 25 June 2010

Abstract

The double inversion recovery (DIR) imaging technique has various applications such as black blood magnetic resonance imaging and gray/white matter imaging. Recent clinical studies show the promise of DIR for high resolution three dimensional (3D) gray matter imaging. One drawback in this case however is the long data acquisition time needed to obtain the fully sampled 3D spatial frequency domain (k-space) data. In this paper, we propose a method to solve this problem using the compressed sensing (CS) algorithm with contourlet transform. The contourlet transform is an effective sparsifying transform especially for images with smooth contours. Therefore, we applied this algorithm to undersampled DIR images and compared with a CS algorithm using wavelet transform by evaluating the reconstruction performance of each algorithm for undersampled *k*-space data. The results show that the proposed CS algorithm achieves a more accurate reconstruction in terms of the mean structural similarity index and root mean square error than the CS algorithm using wavelet transform.

Keywords: Double inversion recovery (DIR); Compressed sensing; Contourlet transform

1. Introduction

The primary application of double inversion recovery (DIR) imaging [1–2] has been black blood imaging [3–4] and neuroanatomic imaging [5]. In gray matter imaging [5–6], which is the focus of our study, sharp contrast is obtained by selectively suppressing the cerebrospinal fluid (CSF) and white matter. Recent work using high resolution three dimensional (3D) DIR imaging has shown its clinical feasibility in the detection of multiple sclerosis lesions [7–8]. Another potential application of 3D DIR gray matter imaging can be studies related to variations of the brain morphometry. For example, using a spin-echo based DIR approach offer more reliability in cortical thickness estimations compared to conventional gradient echo based T1 weighted sequences in regions of main field inhomogeneity [9]. Overall, high resolution 3D DIR imaging can offer a variety of applications. However, to acquire 3D DIR data, a long scan time is typically required.

A common method to reduce data acquisition time is to undersample the spatial frequency domain (*k*-space) data. Various parallel imaging approaches can be used [10–12]. Another approach is to use the compressed sensing (CS) algorithm [13–14]. The CS algorithm has been shown to be powerful undersampling scheme when images can effectively be represented by a sparsifying transform. One of the critical steps here in the reconstruction stage is finding the appropriate sparsifying transform. Previously, sparsifying transforms such as the discrete cosine transform (DCT) or the wavelet transforms have been presented and widely used [14]. In general, wavelet transform shows better reconstruction performance than DCT for magnetic resonance (MR) images and are used frequently as the sparsifying transform [14]. With respect to gray matter DIR images, they are characterized as having semi-sparsity since only the gray matter images are obtained. Another notable feature is the curvy and

* Corresponding author. Department of Electrical and Electronic Engineering, Yonsei University, Seodaemun-gu, Seoul 120-749, South Korea. Tel.: +82 2 2123 5874; fax: +82 2 313 2879.
E-mail address: donghyunkim@yonsei.ac.kr (D.H. Kim).

0730-725X/$ – see front matter
doi:10.1016/j.mri.2010.06.029

corrugated contours coming from the cortex. Overall, the application of CS to DIR can be a promising way to reduce the scan time required. Although sparsifying transforms such as wavelets can be used, one limitation is in the insufficiency in expressing the curve smoothness of DIR gray matter images.

The contourlet transform, first introduced by Do et al. [15], can potentially overcome these limitations. While preserving the sparsifying nature of wavelets, by combining a directional filter bank with a Laplacian pyramid (LP), which is a multiscale decomposition method [16], a directional multiresolution representation for sparse curvy images can be effectively provided [15]. As mentioned, since typical DIR gray matter images are obtained from the cortex regions by suppressing CSF and white matter, the images are semi-sparse with curvy and corrugated contour features making the contourlet transform an effective means for image representation.

In this study, we combine the CS algorithm with the contourlet transform. While the use of the contourlet transform (as a sparsifying transform of the CS algorithm) in general brain MR imaging has been previously presented [17], its full benefit can be appreciated when used with the appropriate image type, such as DIR images.

The overall motivation for this study is to enable high resolution 3D DIR gray matter imaging within clinically feasible scan times with practical undersampled *k*-space data. To verify the efficiency of the proposed algorithm, we perform the comparisons of CS algorithm with conventional wavelet transform under various undersampling ratios using pictures and in vivo data.

2. Materials and methods

2.1. Compressed sensing and the contourlet

CS is an algorithm that reconstructs signal $I \in \mathbb{C}^n$ from its linear measurement $K \in \mathbb{C}^m$ (m < n) and is mathematically expressed as:

$$K = \Phi I \tag{1}$$

Where Φ is the encoding operator. This equation is an underdetermined system, therefore, it is hard to solve this equation. However, under the assumption that I can be sparsely represented in the transform domain (ψI), reconstruction of the signal I from undersampled measurements K is possible by solving a L1-minimization problem.

The CS algorithm used in this study is expressed as:

$$minimize\,|\psi I|_1 + \alpha TV(I),\ s.t.\,|F_u I - K|_2 < \varepsilon \tag{2}$$

as introduced by Lustig et al. [14]. Here ψ represents the sparsifying transform and F_u represents the undersampled Fourier transform which corresponds to the encoding operator in this problem. I is the reconstructed image and K is the obtained *k*-space data. TV denotes the total-variation with its weight α. TV is defined as $TV(I)=\sum_i |D_x(I_i)|+|D_y(I_i)|$, while Dx and Dy represent the derivatives in the x and y directions respectively over the whole image. Eq. (2) is usually solved by an equivalent unconstrained regularization problem [18]

$$arg_I min\left\{ |F_u I - K|_2^2 + \lambda_1 |\psi I|_1 + \lambda_2 \mathrm{TV}(I) \right\}. \tag{3}$$

Here, we used the contourlet transform and wavelet transform as the sparsifying transform. In each case, the same λ_1, λ_2 values, determined empirically, were used. The first order derivative form of total-variation was used.

As mentioned, the wavelet transform's basis has limitations in representing contours because it is constructed from the tensor product of the 1D wavelet basis. However, the contourlet provides different and flexible number of directions at each scale using the LP and directional filter banks offering higher degree of directionality and anisotropy than the wavelet transform [15]. The approximation power of these transforms can be evaluated by the error decay rate using the best M-term approximation. Normally, the best M-term approximation error is defined as $|f - \hat{f}_M|_2^2$, when f is the original signal and $\hat{f}_M$ is the approximated image using only the M-largest coefficients. With this, it has been shown that the wavelet transform has a decay rate of $0(M^{-1})$ [19], while the contourlet transform's decay rate is $0[(logM)^3 M^{-2}]$ [15].

To verify the advantage of using the contourlet transform over the wavelet transform when the images are characterized with contours, we used a "baseball uniform" image as shown in Fig. 1A. Images were reconstructed using the same number of the most significant coefficients (2.5% of the total pixel number) from the sparsifying transform domain of each method.

The reconstruction performance was also compared using simulated and actual k-space data. Using variable density random undersampled *k*-space data, we applied the CS algorithm using both the wavelet and contourlet transform. The "Barbara" image as shown in Fig. 1D was used for the simulations.

Fig. 1. Upper rows shows the reconstructed images using the same number (2.5% of the total pixel number) of the most significant coefficients of the sparsifying transform domain and lower rows shows the reconstructed images assuming a variable density random undersampled k-space data (15% k-space data sampling). (A) Fully sampled reference image. (B) Reconstructed images using wavelet transform. (C) Reconstructed images using contourlet transform. The corrugated stripe features are more clearly visible using the contourlet transform. (D) Reference image that was reconstructed from fully sampled k-space data. (E) Reconstructed image by CS algorithm using wavelet transform. (F) Reconstructed image using proposed algorithm. The stripe features are well preserved with the contourlet transform compared to the wavelet transform.

Reconstructions in this study used a wavelet transform with "9–7" biorthogonal filters with five decomposition levels. For the contourlet transform, we used the same 9–7 filters in the LP stage and the "23–45" biorthogonal quincunx filters in the directional filter bank stage.

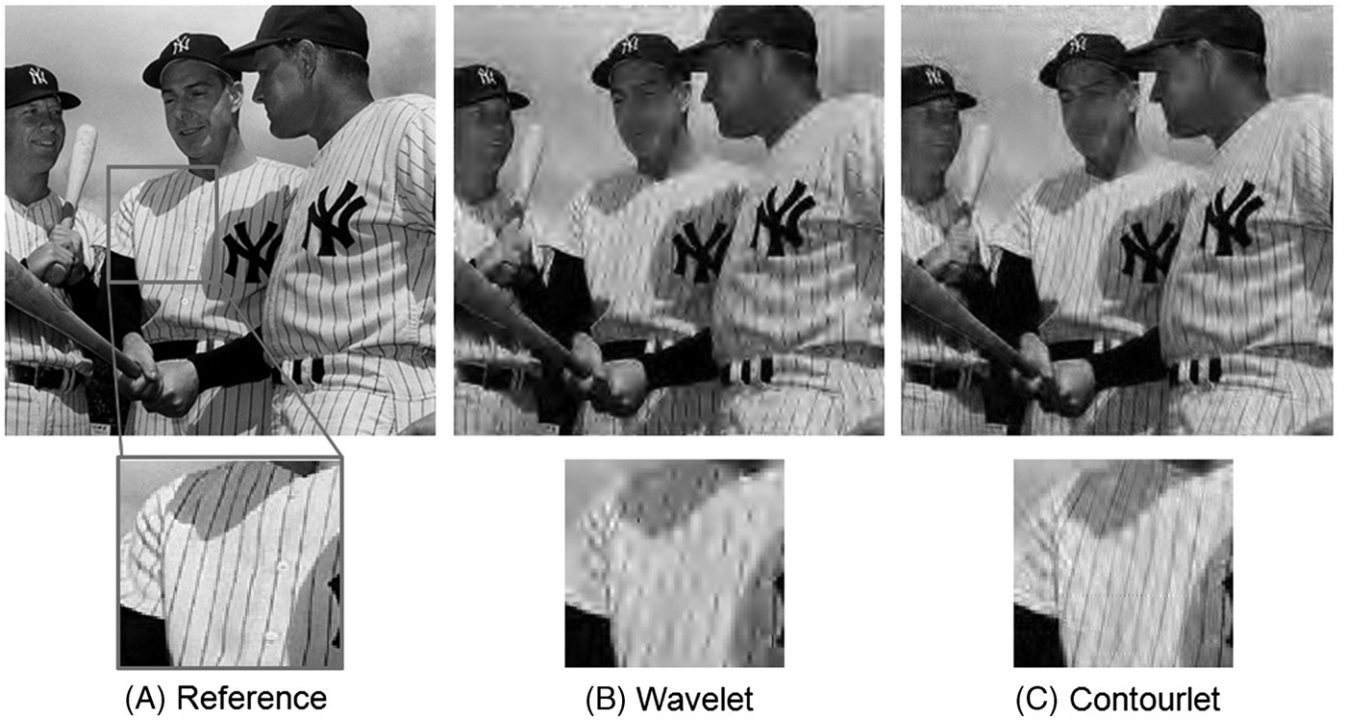

(A) Reference (B) Wavelet (C) Contourlet

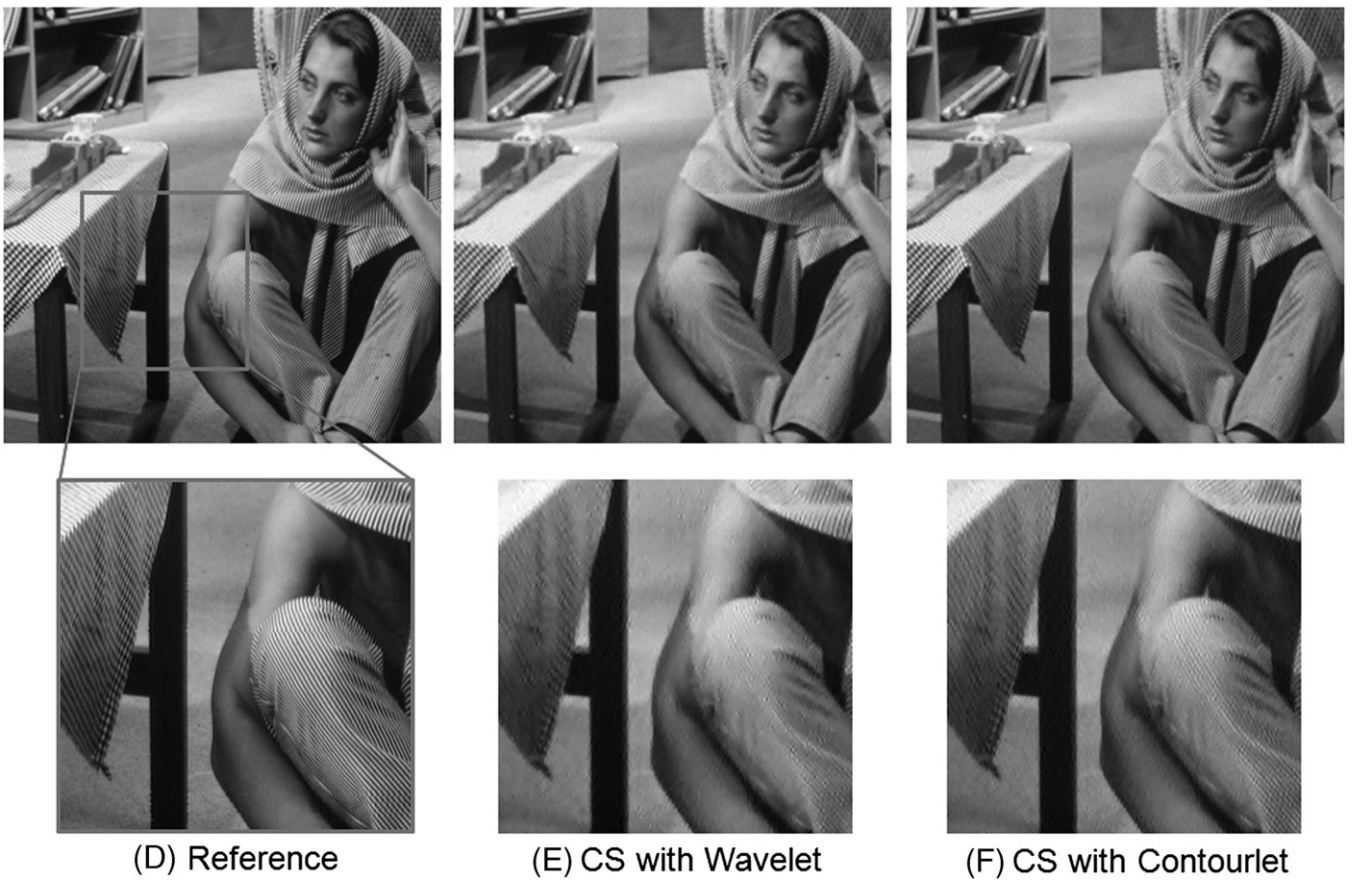

(D) Reference (E) CS with Wavelet (F) CS with Contourlet

All our postprocessing methods were implemented on a PC (Intel Pentium Processor 2.4 GHz, 4 GB of RAM) operating on a Microsoft Windows XP using MATLAB R2007b (Mathworks, Natick, MA, USA).

2.2. In vivo data

In vivo 3D DIR data were collected from eight healthy volunteers using a 3T scanner (Tim Trio, Siemens Medical Solutions, Erlangen, Germany). The 3D DIR sequence uses a variable flip angle turbo spin echo (TSE) imaging scheme [20]. A simplified illustrative representation of the pulse sequence encoding scheme is shown in Fig. 2A. Here, for convenience, we assign G_x as the readout (superior-inferior), G_y as the phase encode (anterior-posterior), and G_z as the slice phase encode (right-left) direction. The number of echoes in an echo-train was set to 188. Random undersampling was performed by arbitrarily choosing select k_z lines from the reference data set as shown in Fig. 2B. No random undersampling was performed in the phase encode direction (i.e., in k_y), rather partial k-space acquisition was used to cover 73.4% of the full k-space, and the resolution of the slice encode direction is 90% as shown in Fig. 2B and C. The other scan parameters were as follows: TR=10000 ms, TE=207 ms, TI1=3651.7 ms (interval between first and second inversion pulses), TI2=551.7 ms (interval between second inversion and excitation pulse), slice thickness=1.0 mm, voxel size=1.0×1.0×1.0 mm, coverage of 25.6×25.6×16.0 cm, total scan time=24 min 2 s for the reference k-space 3D coverage. The institutional review board approved all in vivo studies.

2.3. Quantification instruments of the reconstruction performance

The reconstruction performance was quantified by the mean Structural SIMilarity (MSSIM) index [21] and root mean square (RMS) error. The MSSIM is an image quality assessment metric using luminance, contrast, and structural information. While the RMS error and peak signal-to-noise ratio compare the difference of pixel values between the reference image and reconstructed image, the MSSIM index compares the local patterns of the pixel intensities and have been shown to well represent structural similarities between images. The SSIM index of two images $\bar{x}$ and $\bar{y}$ is defined as

$$\mathrm{SSIM}(\bar{x},\bar{y}) = \frac{\left(2\mu_x\mu_y + c_1\right)}{\left(\mu_x^2 + \mu_y^2 + c_1\right)} \times \frac{\left(2cov_{xy} + c_2\right)}{\left(\sigma_x^2 + \sigma_y^2 + c_2\right)}, \qquad (4)$$

where $\bar{x}$ and $\bar{y}$ are two nonnegative image signals, μ_x and μ_y are the averages of $\bar{x}$ and $\bar{y}$, respectively. cov_{xy} is the covariance of $\bar{x}$ and $\bar{y}$. σ_x^2 and σ_y^2 represent the variances of $\bar{x}$ and $\bar{y}$, respectively. In short, the first term of the right side of the above equation is a luminance comparison term while the second term of the right side represents both contrast and structure comparison term. The constant terms were set to $c_1=(k_1L)^2$ and $c_2=(k_1L)^2$, where L is the dynamic range of the pixel values (e.g., 255 for 8-bit grayscale images), $k_1 \ll 1$ and

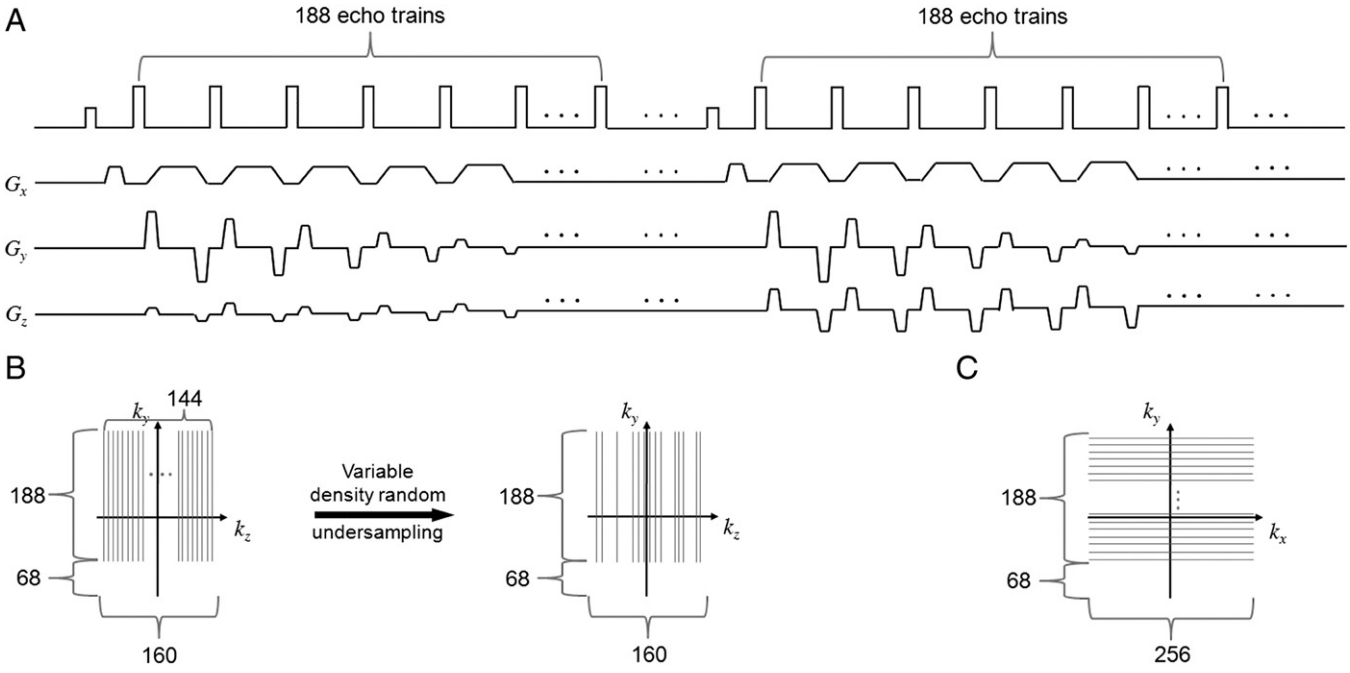

Fig. 2. (A) Simplified 3D DIR pulse sequence encoding diagram. Phase encodes were used in the TSE sequence in k_y and k_z. For our implementation, a reference DIR scan was performed using the sampled coverage as shown in (B) and (C). For undersampled k-space data, the data was selected from the reference coverage as shown in (B). Note that while undersampling in k_z corresponds to reduced scan time, undersampling in k_y does not necessarily reduce the scan time since the TR remains the same.

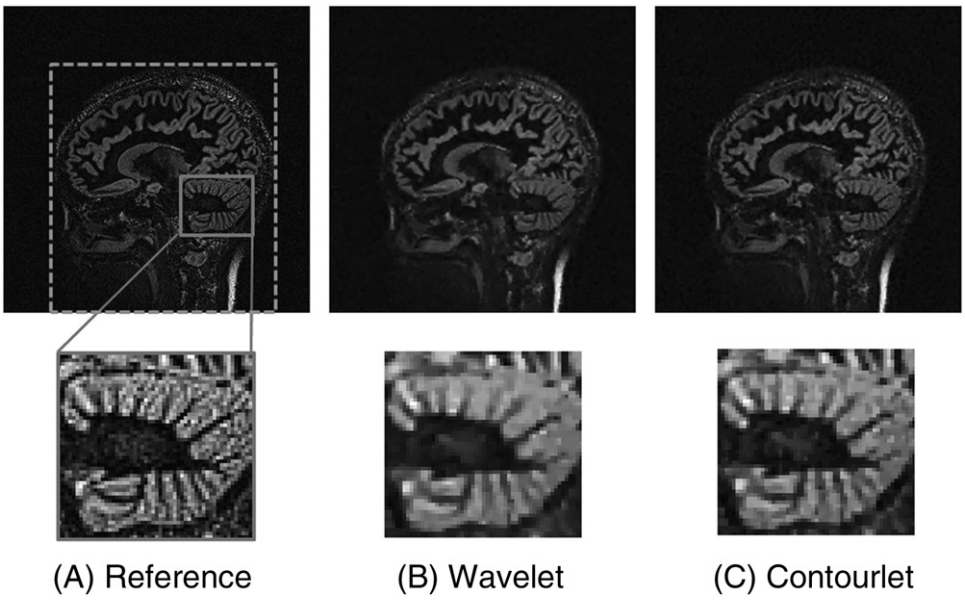

Fig. 3. In vivo images reconstructed using variable density random undersampled k-space data (10% k-space data sampling). (A) Image reconstructed from the reference sampled k-space data. (B) Reconstructed image by CS algorithm using wavelet transform. (C) Reconstructed image using proposed algorithm. The MSSIM index and RMS error in Fig. 4 was calculated from the dotted line box of the reference image using the wavelet transform and contourlet transform.

$k_2 \ll 1$ are small constants (k_1=0.01 and k_2=0.03). The SSIM index was computed within a local 11×11 Gaussian window, which moves pixel-by-pixel over the entire image. The single quality measure MSSIM index used was

$$\mathrm{MSSIM}\left(\overline{X},\overline{Y}\right) = \frac{1}{N}\Sigma_{j=1}^{N}\mathrm{SSIM}\left(\overline{x}_j,\overline{y}_j\right), \tag{5}$$

where $\overline{X}$ and $\overline{Y}$ are the reference image and the reconstructed images, respectively. $\bar{x}_j$ and $\bar{y}_j$ are the image contents at the jth local window and N is the number of local windows of the image. More details regarding the above equations can be found in [21].

RMS error was calculated between the reconstructed image and a reference image.

3. Results

The upper rows in Fig. 1 (A–C) show reconstructed simulation images using the same number of the most significant coefficients (2.5% of the total pixel number)

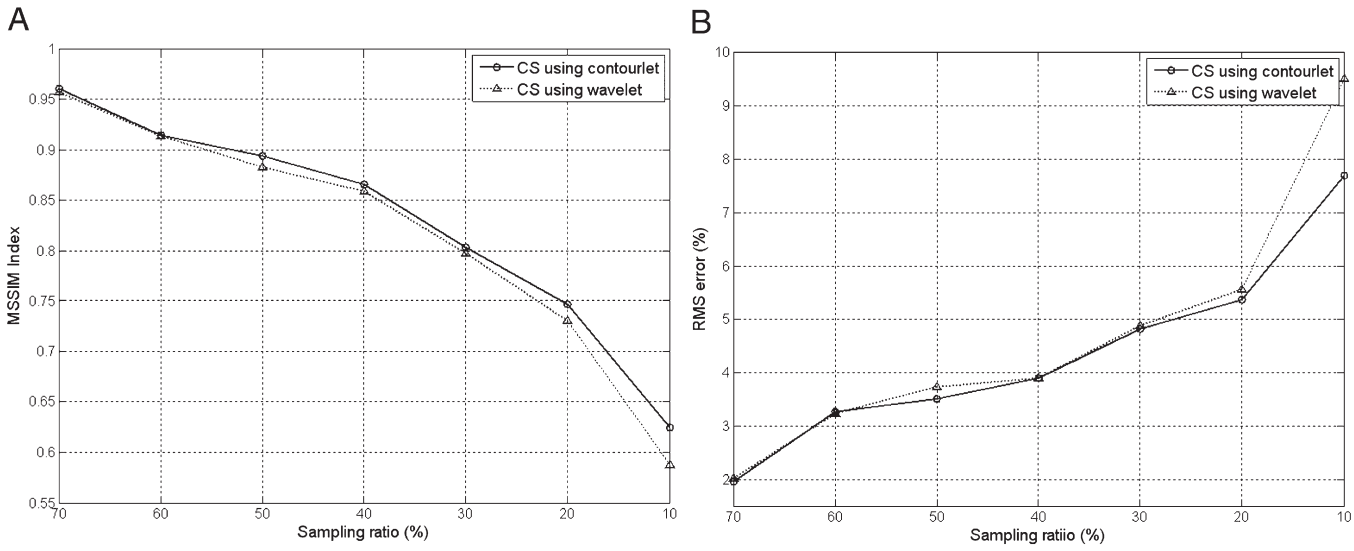

Fig. 4. Change of the MSSIM index values and RMS error values using various k-space sampling ratios. (A) Higher MSSIM values using the CS algorithm with contourlet transform (solid line) compared to the CS algorithm with wavelet transform (dotted line) can be regarded as increased structural similarity. (B) The CS algorithm with contourlet transform compared to the CS algorithm with wavelet transform shows lower RMS error values, i.e., smaller reconstruction error.

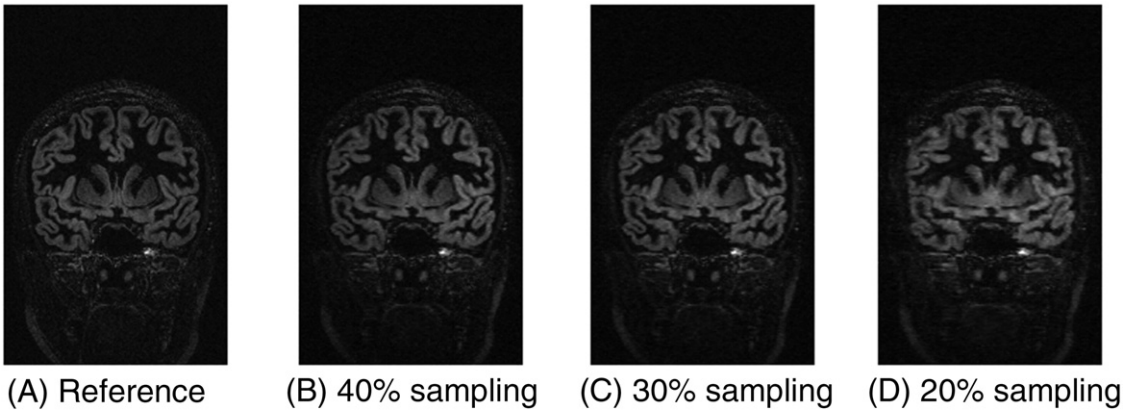

Fig. 5. Reconstructed images by the proposed algorithm using various k-space data sampling ratios. (A) Image reconstructed from reference sampled k-space data. (B) Reconstructed image from 40% sampled k-space data. (C) Reconstructed image from 30% sampled *k*-space data. (D) Reconstructed image from 20% sampled *k*-space data.

from the wavelet and contourlet transform domain. Reconstruction using the contourlet transform shows better resolved images compared to the wavelet transform, especially at the enlarged regions. Reconstructed image using the wavelet transform shows that most of the stripes in the baseball uniform disappear. However, reconstructed image by contourlet transform shows that stripes in the baseball uniform are well represented. This shows that the contourlet transform can better represent images using smaller number of coefficients when the image has smooth contours.

Reconstructed images from simulated variable density random undersampled *k*-space data (15% *k*-space sampling) using CS algorithm with wavelet and contourlet transform are shown in the lower rows of Fig. 1 (D–F). Reconstructed Barbara images using the contourlet transform resulted in higher MSSIM index value and lower RMS error (MSSIM index: 0.7576, RMS error: 5.14%) than CS algorithm using the wavelet transform (MSSIM index: 0.7109, RMS error: 5.50%). Better representation of the curvy features can be seen when using the contourlet transform as the sparsifying transform.

In Fig. 3, reconstructed DIR images using variable density random undersampled *k*-space data (10% *k*-space data) are shown. Reconstructed images using the proposed algorithm resulted in better representation of the curvy features of the cerebellum (at the enlarged region). In Fig. 4, changes in the MSSIM index values and RMS error values for various k-space sampling ratios (70%, 60%,…, 20% and 10%) are shown. The MSSIM index values and RMS error values were estimated from inside the dotted box region of the reference image shown in Fig. 3. The estimated MSSIM index values by the proposed algorithm have larger values than CS algorithm using wavelet transform and the RMS error values shows that the proposed algorithm has smaller errors than CS algorithm using wavelet transform at all undersampling ratios. From these results, it can be seen that DIR gray matter images can more effectively be represented by the contourlet transform than the wavelet transform in terms of its structural similarity. Note here that the undersampling pattern was performed in k_y and k_z from the full data set retrospectively. A limitation to this approach is followed in the discussion section.

Finally in Fig. 5 shows that reconstructed DIR images by the proposed algorithm using various *k*-space data sampling ratios (40%, 30% and 20%) are shown. The expected scan time of some of the undersampling ratios are 9 min 36 s (40%), 7 min 12 s (30%) and 4 min 48 s (20%). As shown, the reconstruction process performs well even for the highly undersampled cases. However, noticeable blurring effects become evident when the sampling ratio is decreased to near 20%.

4. Discussion

One of the important steps in the CS algorithm is applying an appropriate sparsifying transform. Previously, different sparsifying transforms such as DCT, wavelet transform, finite difference with other additional constraints have been applied to the CS equation of Eq. (2) and (3)) for different applications. Here, our goal is to be able to conduct high resolution 3D DIR gray matter imaging within a reasonable scan time. DIR images for gray matter imaging are characterized with having properties such as semi-sparseness, curvy and corrugated features. In these cases, our proposed method of using a contourlet transform as the sparsifying transform shows better reconstruction performance than CS reconstruction using wavelet transform.

As we mentioned, reconstruction of MR images using CS with contourlet transform has been previously proposed [17]. However, a favorable application of using contourlet transform is in images composed of curvy and corrugated features such as DIR images rather than general brain

images. Also, to verify the possibility of using our scheme in real MR data acquisitions, a realizable k-space sampling pattern was assumed, i.e., undersampling in only the phase encoding steps were used.

By using our proposed scheme, it is expected that high resolution 3D gray matter imaging within acceptable scan times can be performed (1 mm^3 full 3D coverage in approximately 7 min). However, we note that one of the major clinical applications of DIR is in the detection of multiple sclerosis [7–8]. For this application, the cortical or mixed gray-white matter lesion might not have contour features making its clinical use limited.

In fact, we expect that our proposed algorithm has other potential applications besides DIR gray matter imaging. For example, angiographic images [22] tend to have curvy and corrugated features. More importantly, there are also various pulse sequence techniques which can enhance the high contrast contour characteristics. Some of these techniques include projection dephaser imaging [23] or tagged images [24]. All of these techniques can benefit using the contourlet transform for applications to rapid imaging or improved reconstruction.

To fully exploit the CS routine with the TSE sequence used in our study, a modification of the pulse sequence to undersample both the k_y and k_z direction would be desired. This is shown in the simulated example of Fig. 3. Here, we limited our undersampling to k_z which can be readily implemented by reducing the number of slice encodes. However, removing echo trains to undersample k_y does not necessarily result in reduced scan time. Presumably, one can undersample both the phase and slice encoding directions simultaneously using a modified view ordering scheme [25]. But, this might cause some unwanted weighting in the collected data resulting in blurring. Further investigation in the pulse sequence modification to fully exploit the 2D undersampling needs to be done.

We have used the RMS error and MSSIM index as metrics. The MSSIM index seems to be a reasonable measure of evaluating the "structural similarity" of images. This metric seems particularly well suited for our application of DIR gray matter imaging since the visual assessment of these semi-sparse images tends to ignore background noise components and focus more on the gray matter structure themselves.

There are various algorithms to reconstruct images from undersampled *k*-space data. Our proposed method can be combined with several of these reconstruction methods. Various parallel imaging reconstruction algorithms [11–12] can be used to achieve further reduction of scan time, which is an active research topic in the field recently [26–28]. Here, we just combined reconstructed images from each coil using sum of square method.

Optimization in the filter parameters can enhance the reconstruction performance. However, finding the optimal filter parameters is difficult. Here we used 9–7 and 23–45 biorthogonal filters which were used in its original study. However, use of more optimal settings (such as kinds of filters and decomposition levels, etc.) can lead to better image reconstruction performance.

5. Conclusion

We have introduced a CS algorithm using the contourlet transform which can be used to alleviate the problem of long scan for high resolution 3D gray matter imaging. Our proposed algorithm improves the reconstruction accuracy (in terms of MSSIM index and RMS error) compared to the CS algorithm using wavelet transforms. We have shown that the proposed algorithm can be an effective method for undersampled sparsifying images characterized with smooth contours. There are many MR images with these characteristics or pulse sequence schemes that enhance these features.

Acknowledgment

This work was supported by the basic research program of the Korea Science and Engineering Foundation (R01–2008–000–20270–0) and by the Ministry of Knowledge Economy and Korea Institute for Advancement in Technology through the Workforce Development Program in Strategic Technology.

References

[1] Redpath TW, Smith FW. Technical note: use of a double inversion recovery pulse sequence to image selectively grey or white brain matter. Br J Radiol 1994;67(804):1258–63.
[2] Turetschek K, Wunderbaldinger P, Bankier AA, Zontsich T, Graf O, Mallek R, et al. Double inversion recovery imaging of the brain: initial experience and comparison with fluid attenuated inversion recovery imaging. Magn Reson Imaging 1998;16(2):127–35.
[3] Song HK, Wright AC, Wolf RL, Wehrli FW. Multislice double inversion pulse sequence for efficient black-blood MRI. Magn Reson Med 2002;47(3):616–20.
[4] Parker DL, Goodrich KC, Masiker M, Tsuruda JS, Katzman GL. Improved efficiency in double-inversion fast spin-echo imaging. Magn Reson Med 2002;47(5):1017–21.
[5] Boulby PA, Symms MR, Barker GJ. Optimized interleaved whole-brain 3D double inversion recovery (DIR) sequence for imaging the neocortex. Magn Reson Med 2004;51(6):1181–6.
[6] Pouwels PJ, Kuijer JP, Mugler III JP, Guttmann CR, Barkhof F. Human gray matter: feasibility of single-slab 3D double inversion-recovery high-spatial-resolution MR imaging. Radiology 2006;241(3):873–9.
[7] Geurts JJ, Pouwels PJ, Uitdehaag BM, Polman CH, Barkhof F, Castelijns JA. Intracortical lesions in multiple sclerosis: improved detection with 3D double inversion-recovery MR imaging. Radiology 2005;236(1):254–60.
[8] Wattjes MP, Lutterbey GG, Gieseke J, Traber F, Klotz L, Schmidt S, et al. Double inversion recovery brain imaging at 3T: diagnostic value in the detection of multiple sclerosis lesions. AJNR Am J Neuroradiol 2007;28(1):54–9.
[9] Yoo E, Park HJ, Kim EY. Unreliability of cortical volumetry in regions near the skull base on 3D T1-weighted imaging: comparison study with 3D double inversion-recovery imaging. Proceedings of

the 16th Annual Meeting of ISMRM. Toronto, Canada: ISMRM; 2008. p. 3502.
[10] Sodickson DK, Manning WJ. Simultaneous acquisition of spatial harmonics (SMASH): Fast imaging with radiofrequency coil arrays. Magn Reson Med 1997;38(4):591–603.
[11] Pruessmann KP, Weiger M, Scheidegger MB, Boesiger P. SENSE: sensitivity encoding for fast MRI. Magn Reson Med 1999;42(5): 952–62.
[12] Griswold MA, Jakob PM, Heidemann RM, Nittka M, Jellus V, Wang JM, et al. Generalized autocalibrating partially parallel acquisitions (GRAPPA). Magn Reson Med 2002;47(6):1202–10.
[13] Donoho DL. Compressed sensing. IEEE Trans Inf Theory 2006;52(4): 1289–306.
[14] Lustig M, Donoho D, Pauly JM, Sparse MRI. The application of compressed sensing for rapid MR imaging. Magn Reson Med 2007;58 (6):1182–95.
[15] Do MN, Vetterli M. The contourlet transform: an efficient directional multiresolution image representation. IEEE Trans Image Process 2005;14(12):2091–106.
[16] Burt PJ, Adelson EH. The Laplacian pyramid as a compact image code. IEEE Trans Commun 1983;31(4):532–40.
[17] Xiaobo Q, Di G, Zhong C, Congbo C. Compressed Sensing MRI based on Nonsubsampled Contourlet Transform. Proceedings of 2008 IEEE International Symposium on IT in Medicine and Education. Xia'men, China: IEEE; 2008. p. 693–6.
[18] Dong L, Bo L, Leslie Y. Accelerating sensitivity encoding using compressed sensing. 30th Annual International IEEE EMBS. Vancouver, Canada: IEEE; 2008. p. 1667–70.
[19] Donoho DL, Vetterli M, DeVore RA, Daubechies I. Data compression and harmonic analysis. IEEE Trans Information Theory 1998;44(6): 2435–76.
[20] Miyati T, Kasai H, Shundo H, Imazawa M, Banno T, Ohba S, et al. Fast RARE MR imaging with variable flip angle excitation. Radiographics 1996;16(3):595–602.
[21] Wang Z, Bovik AC, Sheikh HR, Simoncelli EP. Image quality assessment: from error visibility to structural similarity. IEEE Trans Image Process 2004;13(4):600–12.
[22] Masaryk TJ, Modic MT, Ross JS, Ruggieri PM, Laub GA, Lenz GW, et al. Intracranial circulation: preliminary clinical results with three-dimensional (volume) MR angiography. Radiology 1989;171(3):793–9.
[23] Dixon WT, Du LN, Faul DD, Gado M, Rossnick S. Projection angiograms of blood labeled by adiabatic fast passage. Magn Reson Med 1986;3(3):454–62.
[24] Axel L, Dougherty L. MR imaging of motion with spatial modulation of magnetization. Radiology 1989;171(3):841–5.
[25] Busse RF, Brau AC, Vu A, Michelich CR, Bayram E, Kijowski R, et al. Effects of refocusing flip angle modulation and view ordering in 3D fast spin echo. Magn Reson Med 2008;60(3):640–9.
[26] Zhao C, Lang T, Ji J. Compressed sensing parallel imaging. Proceedings of the 16th Annual Meeting of ISMRM. Toronto, Canada: ISMRM; 2008. p. 1478.
[27] Liu B, Sebert FM, Ying L. SparseSENSE: randomly-sampled parallel imaging using Compressed sensing. Proceedings of the 16th Annual Meeting of ISMRM. Toronto, Canada: ISMRM; 2008. p. 3154.
[28] Liang D, Liu B, Wang JJ, Ying L. Accelerating SENSE using compressed sensing. Magn Reson Med 2009;62(6):1574–84.